Imaging Shear in Sliding Charge-Density Waves by X-Ray Diffraction Topography

Y. Li,[1] S. G. Lemay,[2] J. H. Price,[1] K. Cicak,[2] K. O'Neill,[2] K. Ringland,[2] K. D. Finkelstein,[3]
J. D. Brock,[1] and R. E. Thorne[2]
[1]*School of Applied and Engineering Physics, Cornell University, Ithaca, New York 14853*
[2]*Laboratory of Atomic and Solid State Physics, Clark Hall, Cornell University, Ithaca, New York 14853*
[3]*Cornell High-Energy Synchrotron Source (CHESS), Ithaca, New York 14853*
(Received 17 May 1999)

We have imaged the electric-field-dependent structure of charge-density waves (CDWs) in ribbonlike $NbSe_3$ single crystals by monochromatic x-ray topography. Below the depinning threshold E_T the CDW is well correlated. Just above E_T, the CDW shears along longitudinal steps in crystal thickness associated with small-angle grain boundaries, and at high fields transverse correlations recover. These results demonstrate x-ray topography as an effective probe of superlattice structure and with earlier transport measurements establish that extrinsic sources dominate CDW plasticity observed in $NbSe_3$.

PACS numbers: 71.45.Lr, 61.10.–i, 61.72.Ff

Charge-density waves (CDWs) in quasi-one-dimensional conductors provide one of the most important systems in condensed matter for studying collective dynamics in the presence of disorder. Above a threshold electric field E_T, the CDW depins from impurities and slides relative to the host lattice, producing a nonlinear current-field relation, coherent voltage/current oscillations whose fundamental frequency ν is proportional to the CDW velocity, and a rich variety of other phenomena [1]. Related phenomena are observed in the flux lattices of type-II superconductors [2] and in Wigner crystals [3].

The spatiotemporal dynamics that underlies these phenomena is complex. Early theoretical efforts modeled the CDW as a perfectly elastic periodic medium interacting with random impurities and predicted a sliding state with long-range temporal order [4]. Experimentally, CDWs can show abundant evidence of plasticity especially at fields just above E_T, including broad and complex oscillation spectra and enormous $f^{-\alpha}$ noise. More recent calculations [5] predict field-dependent plasticity that degrades temporal and spatial CDW order in the sliding state. Evaluating these predictions (and related predictions for flux lattices) is problematic because it is often not obvious whether observed plasticity is intrinsic to the dynamics of the randomly pinned periodic medium or instead arises from such extrinsic sources as boundary conditions and chemical or structural inhomogeneities.

We have directly observed field-dependent CDW structure in $NbSe_3$ using x-ray diffraction topography. Above E_T the CDW shears along the longitudinal steps in crystal thickness characteristic of this and many related CDW conductors, and transverse CDW correlations recover somewhat at high fields. Our results demonstrate the potential of x-ray topography as a structural probe of CDWs and other superlattices and establish an important extrinsic source of CDW plasticity.

A CDW consists of a modulation of the conduction electron density of wave vector $Q = 2k_F$ coupled to a lattice distortion $\mathbf{u}(\mathbf{r}, t) = \mathbf{u}_0 \sin[\mathbf{Q} \cdot \mathbf{r} + \phi(\mathbf{r}, t)]$, where ϕ is the phase of the CDW order parameter. X-ray scattering from the distortion produces superlattice peaks displaced from host lattice Bragg peaks by $\pm\mathbf{Q}$. In a macroscopically homogeneous system the line shape of these peaks is related to the CDW's phase-phase correlation function, and the inverse half width at half maximum (HWHM) is proportional to the correlation length [6]. However, when electric fields are applied the CDW's structure may develop large-scale inhomogeneities. For example, above E_T the longitudinal peak width in $NbSe_3$ broadens, and diffraction measurements using a small x-ray beam scanned along the crystal [7] show that this broadening is dominated by a position-dependent shift in CDW wave vector associated with boundary conditions at the current contacts [8,9].

Spatially-resolved structural information can be obtained using x-ray diffraction topography [10], widely used to image defects, domain structure, and structural phase transitions in other materials. In one version of this technique, a crystal is illuminated using a monochromatic, highly parallel x-ray beam and the resulting diffraction pattern recorded using a high-spatial-resolution detector placed very close to the crystal. The x-ray reflections then form images of the crystal, and variations in lattice orientation and spacing within the crystal bulk cause variations in diffracted intensity that produce image contrast. CDW structure has previously been imaged using scanning tunneling microscopy (STM) [11], transmission electron microscopy (TEM) [12], and an indirect scanning electron microscope based technique [13]. STM probes only the crystal surface and is insensitive to the small fractional changes in the CDW wave vector ($<0.1\%$) important in collective pinning and dynamics. TEM perturbs the CDW and host lattice and requires very thin crystals whose properties differ from those of thicker crystals. We have explored x-ray topography because it allows non-perturbing imaging of bulk structure with excellent sensitivity to

 0031-9007/99/83(17)/3514(4)$15.00

lattice distortions and a spatial resolution (a few micrometers) that approaches the x-ray determined static structural correlation lengths of CDWs in the purest crystals [6].

High-purity single crystals (residual resistance ratio $\approx$ 400) of $NbSe_3$—the material that shows by far the cleanest CDW response—were mounted on alumina substrates patterned with a four-probe contact configuration and a 3 mm hole through which the x rays passed and then cooled to $T = 90$ K, below $NbSe_3$'s $T_{P_1} = 145$ K Peierls transition. The CDW's depinning threshold E_T was determined using both differential resistance and I-V measurements, and a helium exchange gas reduced sample heating to less than 1 K for the fields used.

X-ray diffraction measurements were performed on bending magnet station C-2 at the Cornell High-Energy Synchrotron Source using a Ge(111) double-bounce monochromator. The incident beam energy and energy spread were 8.25 KeV and 5 eV and the horizontal and vertical beam divergences were 1.6×10^{-4} and 4×10^{-5} rad, respectively. The crystal was mounted on the Φ axis of a four-cycle diffractometer. Rocking curves were obtained by recording the diffracted intensity as the crystal was rotated about the axis perpendicular to the vertical scattering plane. X-ray topographs were recorded using Kodak Industrex SR film held $\sim$5 cm from the sample and perpendicular to the diffracted beam direction, with exposure times of 2 to 5 min for CDW reflections and 2 to 15 s for lattice reflections. Image sensitivity to in-plane and out-of-plane wave vector rotations was $\sim$0.003° and $\sim$0.01°, respectively.

Figure 1(a) shows optical images of the $\sim 4\ \mu$m $\times$ 30 μm $\times$ 5 mm $NbSe_3$ crystal used for most of this study, and Fig. 1(b) schematically shows this crystal's cross section. Monoclinic $NbSe_3$ crystals have the form of ribbonlike whiskers. The ribbon axis follows the $\mathbf{b}^* = \mathbf{b}$ direction and corresponds to the direction of the T_{P_1} CDW's wave vector $\mathbf{Q_1} \approx 0.243\mathbf{b}^*$ and to the direction of CDW motion [1]. The ribbon thickness corresponds to the $\mathbf{a}^*$ direction and the width to the $\mathbf{c}$ direction [14]. All but perhaps 1 in 10^3 crystals of $NbSe_3$ (and of the related CDW conductors m-TaS_3, o-TaS_3, and NbS_3) have steps on their surfaces that run longitudinally parallel to $\mathbf{b}^*$ and that produce transverse variations in crystal thickness. The crystal in Fig. 1(a) had one large step and a few smaller steps.

Figure 1(c) shows the rocking curve about $\mathbf{b}^*$ for the (0 0 6) reflection of this crystal. Topographs show that the two peaks separated by $\sim$0.075° are due to scattering from regions of the crystal on either side of the large step. The rocking width about $\mathbf{c}$ of the (0 2 0) reflection is a factor of $\sim$8 narrower and is dominated by a slight crystal bending. The crystal steps thus appear to be associated with small-angle boundaries between grains that are well oriented along $\mathbf{b}^*$ but slightly misoriented in the $\mathbf{a}^*$-$\mathbf{c}^*$ plane.

Figure 2(a) shows rocking curves about the $\mathbf{c}$ axis for the (0 1 + Q_1 0) CDW reflection at three different applied fields. Field-dependent variations in the wave vector's

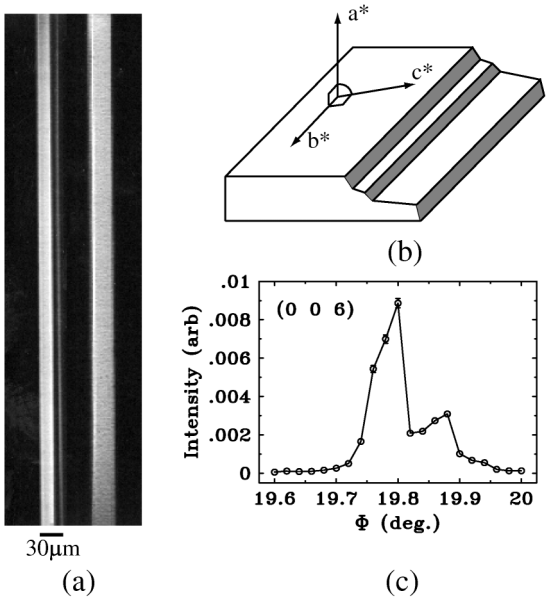

FIG. 1. (a) Optical micrographs along $\mathbf{a}^*$ of the two faces of the $NbSe_3$ crystal studied. (b) Schematic illustration of the crystal cross section. (c) Rocking curve about the $\mathbf{b}^*$ axis of the (0 0 6) Bragg peak.

magnitude were too small to be resolved [7,15] so that the rocking width is determined primarily by wave vector rotations in the $\mathbf{a}^*$-$\mathbf{b}^*$ plane. The curve at zero field consists of a single narrow peak, indicating that the CDW is well correlated in the transverse $\mathbf{a}^*$ direction. When the CDW is depinned the peak's center of mass shifts indicating a rotation of the average wave vector, its width abruptly broadens, and it becomes asymmetric. When the current is reversed the peak shifts in the opposite direction, indicating a rotation in the opposite sense. Figure 2(b) shows the CDW peak HWHM versus driving field obtained from a fit using a convolution of Gaussian and Lorentzian line shapes with equal half-widths. The peak width grows to a maximum at $E \approx 3E_T$ and then narrows to near its $E = 0$ value above $E \approx 7E_T$. Field-dependent transverse CDW

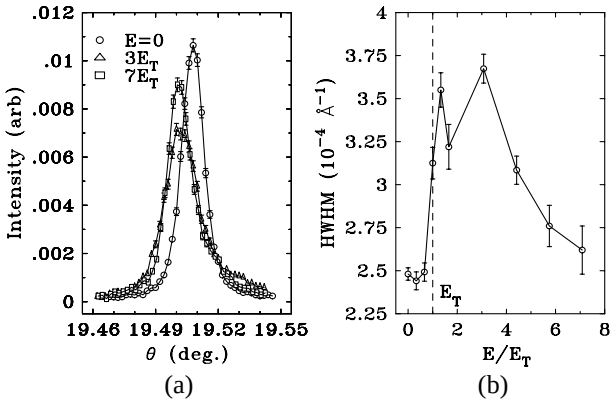

FIG. 2. (a) Rocking curves about $\mathbf{c}$ of the (0 1 + Q_1 0) CDW reflection for three applied electric fields. (b) Rocking curve HWHM versus field. $E_T(T = 90\ \text{K})$ is 50 mV/cm.

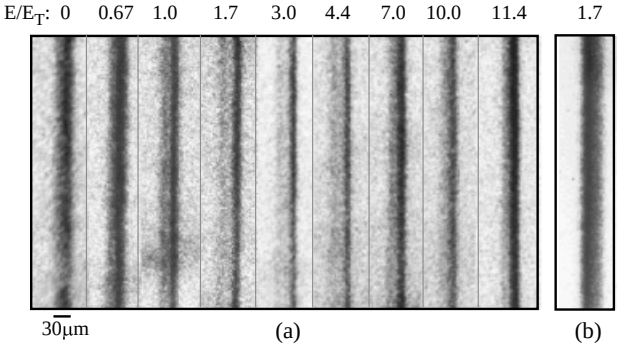

FIG. 3. (a) X-ray topographs of the $(0\ 1 + Q_1\ 0)$ CDW reflection at several applied electric fields. The widths of the crystal images are 30 μm. (b) Topograph of the (0 2 0) Bragg peak at $E = 1.7E_T$.

peak broadenings and shifts have been observed previously in $NbSe_3$ and in $K_{0.3}MoO_3$ [16].

Figure 3(a) shows x-ray topographs of the $(0\ 1 + Q_1\ 0)$ CDW satellite peak at fixed θ and several applied fields. For $E < E_T$, the CDW shows little transverse contrast and is well correlated across the crystal step. For E just above E_T, sharp transverse contrast develops at the largest step due to a decrease in scattered intensity from the thick side of the crystal. As E increases, the width of the reduced intensity region extends into thinner regions of the cross section. Image contrast diminishes beyond $E \approx 4E_T$ and at $E \approx 11E_T$ is only slightly stronger than at $E = 0$, consistent with the narrowing of the rocking width in Fig. 2. Topographs of the (0 2 0) Bragg reflection [Fig. 3(b)] show no contrast variation with applied field. Figure 4 shows topographs of the CDW acquired at fixed current and different rocking angles θ. Regions on opposite sides of the step diffract most strongly at different angles and thus contribute to different parts of the CDW's rocking curve.

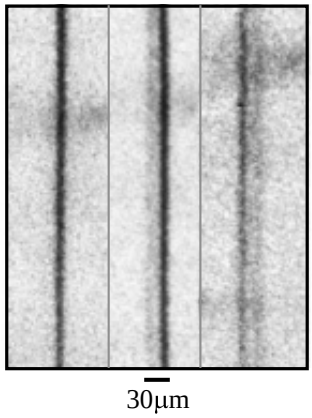

FIG. 4. Topographs of the $(0\ 1 + Q_1\ 0)$ CDW reflection at $E = 1.7E_T$ and $\theta = \theta_{cen} - \text{HWHM}$, $\theta = \theta_{cen}$, and $\theta = \theta_{cen} + \text{HWHM}$, where θ_{cen} and HWHM are determined from the rocking curve in Fig. 2(a). The off-peak image exposure times are double those for the on-peak image.

Image contrast can result from changes in the magnitude of the CDW wave vector, corresponding to longitudinal CDW strains, and from changes in the wave vector's direction, corresponding to shear strains. Evidence for longitudinal strains arising from boundary conditions at current contacts [7–9] was observed in preliminary x-ray images acquired using a somewhat higher resolution setup, but these strains could not be resolved in the present measurements. The effects of shear strains on image contrast depend upon the direction of rotation of the CDW wave vector. In our experiments with scattering in the $\mathbf{a}^*$-$\mathbf{b}^*$ plane, rotations within the scattering plane change the scattered intensity at fixed θ and can be mapped out by acquiring topographs at different θ values within the reflection's rocking curve. Rotations perpendicular to the scattering plane cause scattering to be deflected sideways, reducing the intensity at the corresponding position in the image formed in the absence of such rotations. The variation in image contrast with rocking angle in Fig. 4 and the reduction in rocking curve area (measured with finite transverse detector aperture) in Fig. 2 indicate the presence of both in-plane and out-of-plane wave vector rotations, respectively, for $E > E_T$.

We believe that these wave vector rotations and associated image contrast result when the CDW shears along thickness steps as a consequence of differences in the strength of CDW pinning on either side. The depinning field E_T in undoped $NbSe_3$ varies inversely with crystal thickness in all but the largest crystals that can be grown [17,18]. This size dependence results because collective pinning in $NbSe_3$ is weak and bulk CDW correlations are limited by the crystal thickness so that pinning is two dimensional [6,18]. Consequently, CDW motion first occurs on the thicker side when its smaller depinning field is exceeded. The CDW shears from the thinner, more strongly pinned side, causing bending of the CDW wave fronts in the thick region as shown in Fig. 5(a) and an out-of-plane rotation of the average CDW wave vector. Since only the lower portion of the thick side in Fig. 1(b)

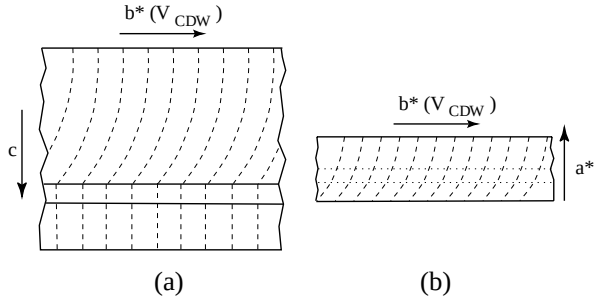

FIG. 5. Schematic illustration of (a) out-of-plane and (b) in-plane deformations for scattering in the $\mathbf{a}^*$-$\mathbf{b}^*$ plane associated with CDW shear along the thickness step for $E > E_T$, as viewed from above and from the left side, respectively, in Fig. 1(b). Dashed lines indicate CDW wave fronts, which are perpendicular to the local CDW wave vector.

directly experiences friction with the thin side, the CDW wave fronts on the thick side also bend as shown in Fig. 5(b), causing an in-plane wave vector rotation. At large fields the entire cross section is depinned, and transverse CDW correlations recover when the difference in pinning forces across the width becomes small compared with the applied force.

The present results are consistent with those of Maher *et al.* [19], who found that $NbSe_3$ crystals with one large thickness step exhibited large amplitude $f^{-\alpha}$ noise and coherent oscillation spectra with a split fundamental. When such crystals were cleaved lengthwise along the step, the resulting nearly rectangular cross-section crystals showed dramatically reduced $f^{-\alpha}$ noise and much sharper oscillation spectra. This difference was attributed to CDW shear occurring along the steps.

Recent theoretical calculations for driven CDWs [5] predict a plastic flow regime just above E_T and a transition to a more ordered moving elastic solid state at high fields. At first sight, these predictions appear qualitatively consistent with transport experiments on nearly all $NbSe_3$ crystals and on a variety of other CDW materials, and with the field-dependent rocking curves in Fig. 2. However, the extremely rare crystals of $NbSe_3$ that are nearly thickness-step-free show dramatically more coherent transport at all fields above E_T [20] and their much smaller diffraction line widths do not narrow at high fields as in Fig. 2, indicating that CDW shear dominates the behavior of ordinary crystals. The coherence of step-free crystals does improve continuously with increasing field and degrades with decreasing temperature [20], but these effects are at least approximately consistent with the plasticity and observed longitudinal variation in CDW current density associated with CDW-to-single particle current conversion near current contacts [9]. Consequently, we conclude that the plasticity observed in $NbSe_3$ and likely also in all other CDW materials is dominated by extrinsic sources and that more realistic calculations are required to convincingly evaluate the apparently more subtle effects of intrinsic plasticity. Even so, the prospects for quantitative understanding of intrinsic plasticity in CDW conductors may be brighter than in flux lattices, where a much smaller shear elasticity combined with generally greater material inhomogeneity seem likely to make compelling comparisons between theory and experiment difficult indeed.

We acknowledge fruitful conversations with S. Kycia and W. W. Webb. This research was supported by the NSF (DMR-97-05433 and DMR-98-01792).

[1] See review articles by P. Monceau, G. Gruner, and J. P. Pouget, in *Physics and Chemistry of Low-Dimensional Inorganic Conductors*, edited by C. Schlenker *et al.* (Plenum, New York, 1996).
[2] G. Blatter *et al.*, Rev. Mod. Phys. **66**, 1125 (1994).
[3] E. Y. Andrei *et al.*, Phys. Rev. Lett. **60**, 2765 (1988).
[4] H. Fukuyama and P. A. Lee, Phys. Rev. B **17**, 535 (1978); P. A. Lee and T. M. Rice, *ibid.* **19**, 3970 (1979); L. Sneddon, M. C. Cross, and D. S. Fisher, Phys. Rev. Lett. **49**, 292 (1982); H. Matsukawa and H. Takayama, J. Phys. Soc. Jpn. **56**, 1507 (1987); A. A. Middleton and D. S. Fisher, Phys. Rev. B **47**, 3530 (1993); C. R. Myers and J. P. Sethna, *ibid.* **47**, 11 171 (1993).
[5] L. Balents and M. P. A. Fisher, Phys. Rev. Lett. **75**, 4270 (1995); V. M. Vinokur and T. Nattermann, *ibid.* **79**, 3471 (1997); L. Balents, M. C. Marchetti, and L. Radzihovsky, Phys. Rev. B **57**, 7705 (1998).
[6] R. M. Fleming *et al.*, Phys. Rev. B **30**, 1877 (1984); D. DiCarlo *et al.*, Phys. Rev. B **50**, 8288 (1994).
[7] D. DiCarlo *et al.*, Phys. Rev. Lett. **70**, 845 (1993); H. Requardt *et al.*, Phys. Rev. Lett. **80**, 5631 (1998).
[8] D. Feinberg and J. Freidel, J. Phys. (Paris) **49**, 485 (1988); J. C. Gill, in *Physics and Chemistry of Low-Dimensional Inorganic Conductors* (Ref. [1]), p. 411; M. E. Itkis, B. M. Emerling, and J. W. Brill, Phys. Rev. B **52**, R11 545 (1995).
[9] T. L. Adelman *et al.*, Phys. Rev. B **52**, R5483 (1995); S. G. Lemay *et al.*, *ibid.* **57**, 12 781 (1998).
[10] B. K. Tanner, *X-ray Diffraction Topography* (Pergamon, Oxford, 1976).
[11] C. G. Slough *et al.*, Phys. Rev. B **39**, 5496 (1989); G. Gammie *et al.*,, Phys. Rev. B **40**, 11 965 (1989); I. B. Altfeder and S. V. Zaitsev Zotov, *ibid.* **54**, 7694 (1996).
[12] K. K. Fung and J. W. Steeds, Phys. Rev. Lett. **45**, 1696 (1980); C. H. Chen, R. M. Fleming, and P. M. Petroff, Phys. Rev. B **27**, 4459 (1983).
[13] G. Heinz *et al.*,, Phys. Lett. A **236**, 583 (1997).
[14] $\mathbf{a}^*$, $\mathbf{b}^*$, and $\mathbf{c}^*$ are vectors of the reciprocal lattice.
[15] The x-ray beam illuminated roughly the middle third of the region between current contacts. The contact-related longitudinal CDW strains there should be less than 0.05%, smaller than the $\sim 0.1\%$ resolution of the present experiment.
[16] J. Zhang, J. F. Ma, S. E. Nagler, and S. E. Brown, Phys. Rev. B **47**, 1655 (1993); K. L. Ringland *et al.*, Phys. Rev. Lett. **82**, 1923 (1999).
[17] D. V. Borodin, F. Ya. Nad, S. Savistkaja, and S. V. Zaitsev-Zotov, Physica (Amsterdam) **143B**, 73 (1986); P. J. Yetman and J. C. Gill, Solid State Commun. **62**, 201 (1987).
[18] J. McCarten *et al.*, Phys. Rev. B **46**, 4456 (1992).
[19] M. P. Maher *et al.*, Phys. Rev. B **43**, 9968 (1991).
[20] R. E. Thorne *et al.*, Phys. Rev. B **35**, 6348 (1987).